Three-dimensional resistivity tomography of Vulcan's forge, Vulcano Island, southern Italy

A. Revil, T. C. Johnson, Anthony Finizola

Three-dimensional resistivity tomography of Vulcan's forge, Vulcano Island, southern Italy

A. Revil,[1,2] T. C. Johnson,[3] and A. Finizola[4]

[1] 9,525 DC resistivity measurements were taken along 9 profiles crossing the volcanic edifice of La Fossa di Vulcano (the forge of God Vulcan in ancient Roman mythology), Vulcano Island (Italy) using a total of 958 electrode locations. This unique data set has been inverted in 3D by minimizing the L_2 norm of the data misfit using a Gauss-Newton approach. The true 3D inversion was performed using parallel processing on an unstructured tetrahedral mesh containing 75,549 finite-element nodes and 398,208 elements to accurately model the topography of the volcanic edifice. The 3D tomogram shows a very conductive body (>0.1 S/m) comprised inside the Pietre Cotte crater with conductive volumes that are consistent with the position of temperature and CO_2 anomalies at the ground surface. This conductive body is interpreted as the main hydrothermal body. It is overlaid by a resistive and cold cap in the bottom of the crater. The position of the conductive body is consistent with the deformation source responsible for the observed 1990–1996 deflation of the volcano associated with a decrease of hydrothermal activity. **Citation:** Revil, A., T. C. Johnson, and A. Finizola (2010), Three-dimensional resistivity tomography of Vulcan's forge, Vulcano Island, southern Italy.

1. Introduction

[2] DC electrical resistivity imaging is a simple yet powerful technique to image and monitor active volcanoes and hydrothermal systems because resistivity is sensitive to porosity, water content, alteration (cation exchange capacity), salinity (TDS), and temperature [*Revil et al.*, 2002, 2004, 2008; *Legaz et al.*, 2009]. Vulcano is an active volcanic island (3 × 7 km) located at the southernmost of the Aeolian Islands in the Tyrrhenian Sea in Italy (38°24′N, 14°58′E) along a major NW–SE tectonic fault named the Tindari-Letojanni fault. This fault crosses Sicily and the islands of Vulcano and Lipari and is associated with secondary faults, craters and volcanic tectonic depressions on these two islands (Figure 1a). On Vulcano island, La Fossa cone is a modest volcanic edifice located in its northern sector. It was formed in the last 6 Ky and gave its name to the "vulcanian" type of explosive activity. In the Roman mythology, Vulcano was considered to be the chimney to the forge of Vulcan (Hephaistos), the blacksmith of the roman gods. The activity of this volcanic island is characterized by both explosive phreatic eruptions and eruptions producing pumice fall deposits and lava flows. The morphology of La Fossa cone have been structured through five main periods of activity: Punte Nere, Palizzi, Forgia Vecchia, Pietre Cotte, and Gran Cratere (Figure 1b) [*Frazzetta et al.*, 1983]. Since its last eruption (1888–1890), Vulcano has been affected by two fumarolic crisis. The first one occurred in 1913–1923. The second episode began in 1977 and lasts until nowadays. During this last fumarolic activity, magmatic fluid inputs have been evidenced by the geochemistry of the fumaroles in 1979–1981, 1985, 1988, 1996, and 2004–2005 in association with swarms of seismic events. Since 1977, the temperature progressively increased and reached 690°C in May 1993.

[3] Because of its dimensions and accessibility, this edifice has been a natural laboratory for geochemists, volcanologists and geophysicists interested to understand magmatic hydrothermal systems [*Granieri et al.*, 2006; *Blanco-Montenegro et al.*, 2007]. In the present letter, we performed a 3D Gauss-Newton inversion of the resistivity data presented by *Revil et al.* [2008] and we discuss the resulting tomogram in terms of localization of the hydrothermal body, fumarolic vents, and tectonic features. This is the first time that a true 3D resistivity inversion is performed over a volcanic edifice (usually inversions of DC or MT data are 1D or 2D with an interpolation between the inverted data to form a pseudo-3D dataset of resistivity).

2. Data Acquisition and Inversion

[4] Resistivity data were measured in October 2005, May 2006, and October 2006 along nine profiles including roll-overs of the electrodes with a total of 9,525 resistivity measurements (Figure 2). We use a set of 64 brass electrodes with a take-out of 20 meters and a cable of 1.26 km. Each of these 9,525 resistivity measurements represents actually the mean of 8 to 16 distinct measurements stacked together with the same set of AB(current)-MN(potential) electrodes. Contact between the electrodes and the ground was improved by adding salty water at each electrode location but it was difficult, most of the time, to inject more than 50 mA in the ground. We used the Wenner-α array for its good signal-to-noise ratio. The temperature measurements reported in Figure 2 were performed at a depth of 30 ± 2 cm [*Revil et al.*, 2008; *Barde-Cabusson et al.*, 2009]. This dataset was merged with the detailed grid temperature measurements performed with the same approach in August 1996 inside the crater of La Fossa cone by *Aubert et al.* [2008]. Thanks to a multi-sensor permanent monitoring station at Stromboli volcano,

[1]Department of Geophysics, Colorado School of Mines, Golden, Colorado, USA.
[2]LGIT, UMR 5559, Université de Savoie, INSU, CNRS, Le Bourget-du-Lac, France.
[3]Energy Resource Recovery and Management, Idaho National Laboratory, Idaho Falls, Idaho, USA.
[4]Laboratoire GéoSciences Réunion, UMR 7154, UR, IPGP, Saint-Denis, La Réunion.

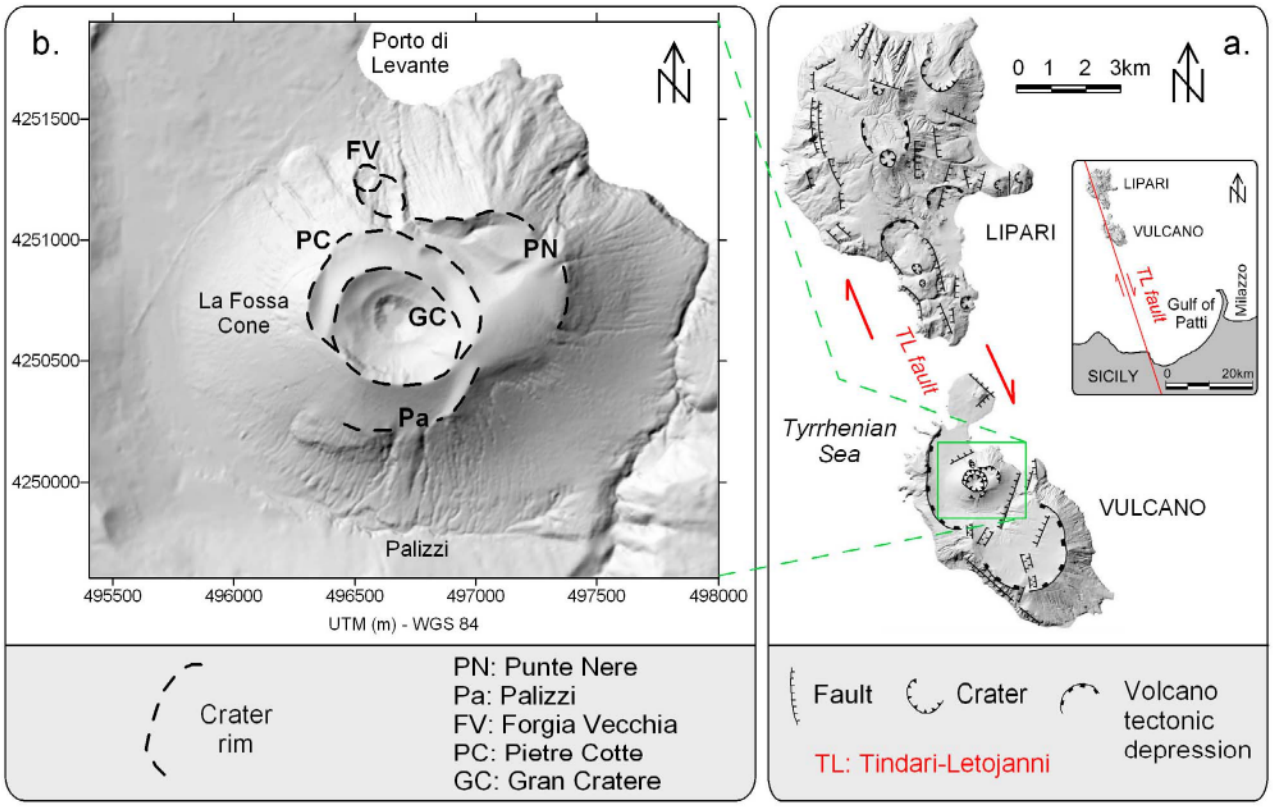

Figure 1. Map of the Island of Vulcano (Italy) and its tectonic context. (a) Main tectonic fault system crossing the Vulcano and Lipari islands (from *Mazzuoli et al.* [1995] and modified by *Gioncada et al.* [2003]). (b) Location of the main crater rims of La Fossa Cone (modified from *Frazzetta et al.* [1983]). The digital elevation map of Vulcano is from *Baldi et al.* [2002].

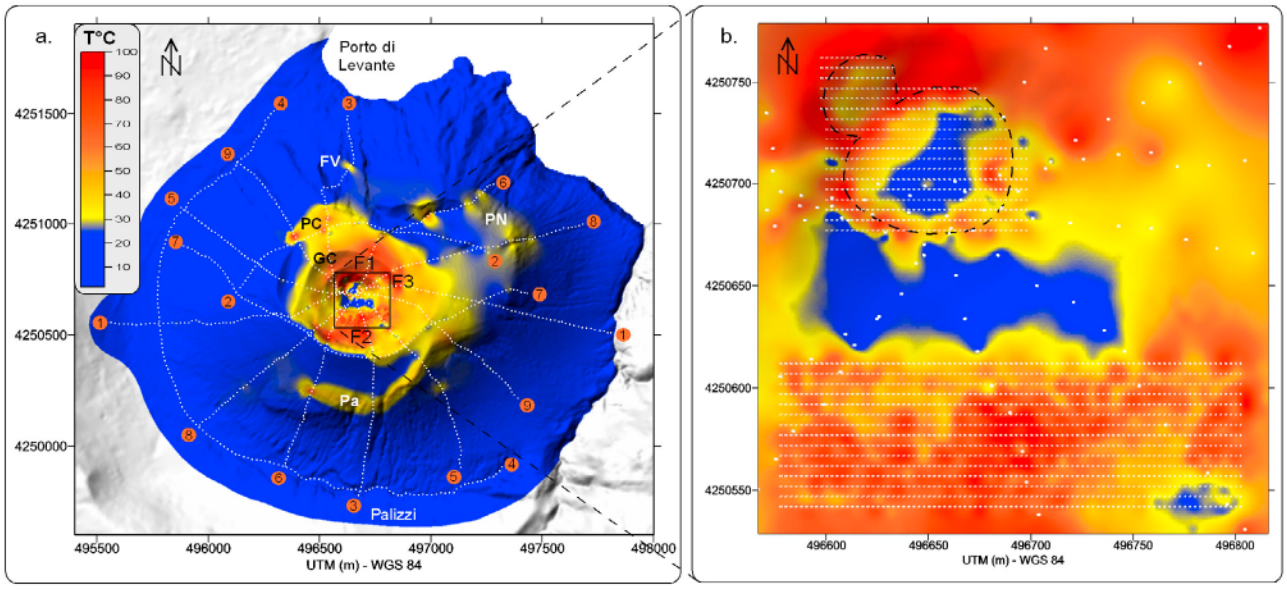

Figure 2. Temperature map at a depth of 30 cm. (a) Temperature map of La Fossa di Vulcano with the position of the resistivity profiles (labeled 1 to 9, see the small white dots) and the 958 electrodes locations (the small white dots). The temperature map was obtained merging our thermal data set with the 2392 measurements performed by *Aubert et al.* [2008]. (b) Zoom in the inner part of the crater. The smaller white dots come from *Aubert et al.* [2008] and the larger one from our study. The black dashline indicates the bottom of the crater. Note the cold temperature at the bottom of the crater. F1, F2, and F3: location of the main fumarolic areas. Other symbols: same as Figure 1.

a protocol of correction has been established to correct the 1996 measurements from the seasonal temperature changes. The combined temperature maps (Figure 2) provides an independent verification of the hydrothermal activity in the vicinity of the ground surface.

[5] The forward modelling resistivity code solves Poisson equation for the electrical potential with the finite element method using the formulation of *Rücker et al.* [2006]. We consider resistivity as scalar and not as a second order symmetric tensor (therefore the assume isotropy of the material). We first computed the pole solution for each electrode used as a current source or sink. The potential distribution for a dipole AB source/sink current pair is then constructed by subtracting the pole potential associated with the current sink. We implemented this true 3D inversion approach in a parallel environment using 480 processors on the Icestorm cluster located at the Idaho National Laboratory. The processors are organized in a "master/slave" configuration where one node serves as the master node, which controls execution of the program and instructs slaves concerning which routines to execute. A complete description of the parallel inversion algorithm is given by *Johnson et al.* [2010].

[6] The inversion minimizes an objective function, which is the sum of the L_2 norm of the weighted data misfit and the L_2 norm of the model regularization error. The regularization operator is formulated so that the regularization error increases as the estimated conductivity structure deviates from homogeneity. Therefore, the value of the objective function is governed by a trade-off between honoring the weighted resistivity data (which impose heterogeneity), and honoring the regularization constraints (which impose homogeneity). The relative importance placed upon these competing objectives is governed by the regularization or trade-off parameter, which scales the regularization term of the objective function. The trade-off parameter is initially set to a large value thereby imposing homogeneity in the inverse solution, and then decreased as the algorithm progresses to allow heterogeneity sufficient only to honor the weighted resistivity data. Thus, the only heterogeneity displayed in the final solution is that which the resistivity data are able to resolve. The individual resistivity data are weighted according to data noise using a data weighting matrix. The objective function is minimized with the Gauss-Newton algorithm as described by *Johnson et al.* [2010].

[7] To construct the mesh, known topography was used over the survey area and extrapolated further away to avoid edge effects. The computational mesh consists of 958 electrode locations, 75,549 finite-element nodes, and 398,208 tetrahedral elements. The relatively large number of elements with respect to the number of data in this case was required to accurately model the complicated surface topography. However, it should be kept in mind that model resolution at a particular scale is not a function of the number of elements in the model. It is a function of the information provided by the data. The inverse computations were conducted on 480 nodes (1 master and 479 slave nodes), requiring approximately 2 hours (26 Gauss-Newton iterations) for convergence. Convergence criteria are generally set based upon data error. That is, when the L_2 norm of the data misfit reduces to a value that is consistent with the estimated data noise, the inverse solution is assumed to have converged.

3. Interpretation

[8] The electrical resistivity tomogram resulting from the inversion is shown in Figures 3b–3d (see also auxiliary material).[1] A histogram of the data misfit for the inverse solution is shown in Figure 3e. Here the error is defined as the residual normalized by the observed value. With respect to a normal distribution, the error histogram displays elongated tails. These are likely due to the low level of current injected into the volcano, as explained above, and resulting noisy data. Because there are no cross-line measurements between the 9 profiles, the surface resistivity structure is uncertain in many areas and may contain artifacts. The deeper structure is better resolved especially in the central part of the edifice. The resistivity tomogram shows a correspondence between the high conductivity areas (>0.1 S/m) and the position of the main surface temperature anomalies evidenced by thermal infrared images of *Chiodini et al.* [2005, Figure 1a], or in a detailed soil temperature study at 30 cm depth [*Aubert et al.*, 2008] coupled with our dataset (see Figure 2b). Figure 2b clearly evidences cold temperatures at the bottom of the present crater. This thermal characteristic is also consistent with the CO_2 anomaly distribution described by *Granieri et al.* [2006, Figure 2]. This high conductivity subvolume is therefore associated to the high temperature of the hydrothermal fluids (>200°C) evidencing high permeability pathways. However the presence of a magnetized body inside the Fossa cone [*Blanco-Montenegro et al.*, 2007] implies that high temperatures are contained in very limited spaces and do not affect its bulk inner structure. Additional contributions to high conductivity could come from alteration and salinity of the brines.

[9] The volume of the high conductivity body at depth is less than 0.1 km^3 in agreement with the size of the hydrothermal system inferred by *Italiano et al.* [1984] using mass balance calculations and is comprised inside the Pietre Cotte crater. The position of this body is also in agreement with the subvertical prolate spheroidal source inferred by *Gambino and Guglielmino* [2008] from the observed 1990–1996 deflation of La Fossa di Volcano. This reinforces their interpretation that the fluid loss from the shallow hydrothermal reservoir shown in Figure 3b was the most likely cause of the subsidence recorded at La Fossa Cone during the period 1990–1996. Indeed, the maximum of temperature occurring in May 1993 could be interpreted as a consequence of the last magmatic input in 1988, which pressurized the hydrothermal system, and the consequent release of the fluid pressure and the associated deflation of the edifice during the period 1990–1996. In 1996, a new magmatic input pressurized again the system.

[10] The fumaroles observed at La Fossa cone are a mix of a gas contribution released from a magma body (~2.5 km depth [*Nuccio and Paonita*, 2001]) and a shallower one formed by the evaporation of brines of marine origin [*Granieri et al.*, 2006]. We note a strong difference in the pattern and value of the electrical conductivity between the SN profile (Figure 3d)

[1] Auxiliary materials are available in the HTML. doi:10.1029/2010GL043983.

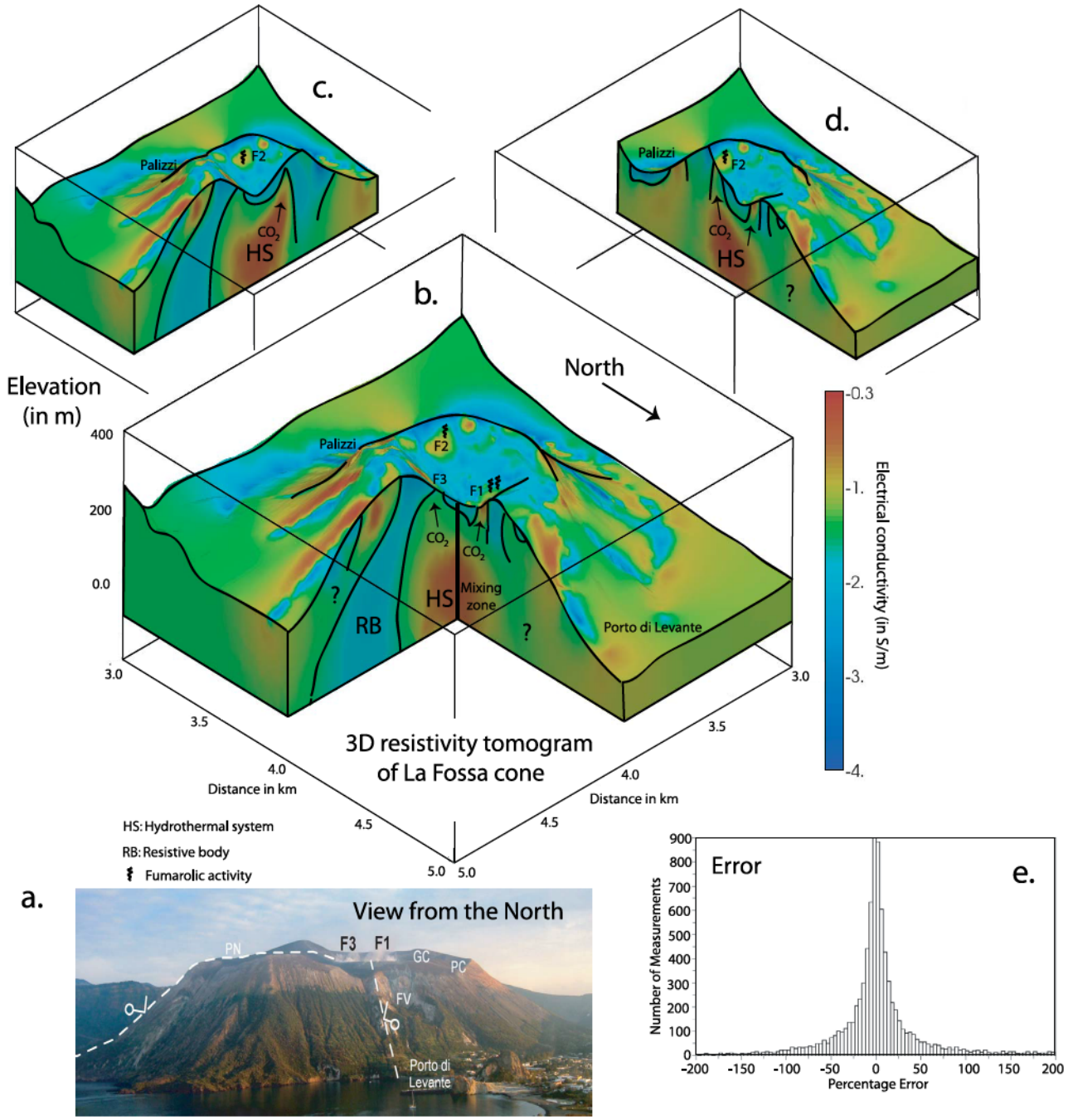

Figure 3. 3D resistivity tomogram of La Fossa di Vulcano using the log of the electrical conductivity. (a) Picture taken from the North. Craters: PN, Punte Nere; FV, Forgia Vecchia; PC, Pietre Cotte; GC, Gran Cratere. F1, F2, and F3: areas of intense fumarolic activity. (b–d) Resistivity tomogram and its interpretation (vertical exaggeration 2:1). Note the asymmetry of the conductivity distribution between the EW and SN profiles. (e) Percentage error distribution.

and the EW profile (Figure 3c). The EW profile shows resistive bodies on the flank of the volcano. The SN profile is more conductive. This is an expected as the growth of Vulcano is controlled by the NW–SE, Tindari–Letojanni strike-slip faults and by the associated N–S striking normal faults (Figure 1a). Moreover, this SN profile also crosses higher permeability areas corresponding to old crater boundaries used as drains by hydrothermal fluids (Forgia Vecchia on Northern flank and Palizzi on Southern flank (Figures 1b and 2)). The resistive body on the eastern side of the volcano has been interpreted as an old dome structure by *Barde-Cabusson et al.*, [2009].

[11] The 3D resistivity tomogram could be used also to assess the CO_2 plumbing system of the volcano as CO_2 flux anomalies recorded at the ground surface are also consistent with the position of the conductivity anomaly. DC resistivity is therefore a useful information if we want to model, with a reactive transport code, the CO_2 flux changes observed at the

ground surface by *Granieri et al.* [2006] and corresponding to increase volatile release from a stationary magma system. The anomaly F1 in Figure 3 corresponds to the position of the main fumarolic field. The anomaly F2 and F3 corresponds also to areas of thermal and CO_2 anomalies. These surface anomalies can be extended downward to the main hydrothermal body. It would be very interesting in future measurements to assess how DC resistivity tomography could be used to assess changes in the hydrothermal system like its temperature and the CO_2 content. A correlation between these changes and the seismicity, the magmatic input, and the deformation of the edifice would be of the first interest. The aim would be to better constrain the influence of the hydrothermal system of La Fossa regarding unrest and eruptive events.

4. Conclusions

[12] We performed a true 3D resistivity tomography of La Fossa di Vulcano (Aeolian Islands, Italy) using a non-linear Gauss-Newton algorithm and parallel programming. Time lapse DC and complex resistivity tomography are expected to increase our conceptual understanding of the architecture of active volcanoes in coming years and will offer a powerful method to monitor the fundamental chemicohydromechanical processes occurring in magmatic hydrothermal systems. In the case of La Fossa di Vulcano, joint inversion of DC resistivity with magnetic and gravity data could help to get a clearer picture of the geology and tectonic features affecting this edifice and reduce the inherent non-uniqueness of potential field methods.

[13] **Acknowledgments.** Financial support was provided by DOE (award GO18195), INSU-CNRS, the Laboratoire GéoSciences Réunion (France), CNR, INGV, and the Dipartimento per la Protezione Civile (Project V3.5 Vulcano, 2005–2007) in Italy. We thank S. Piscitelli, E. Rizzo, T. Ricci, A. Angeletti, A. Crespy, M. Balasco, S. Barde Cabusson, L. Bennati, S. Byrdina, N. Carzaniga, F. Di Gangi, J. Morin, A. Perrone, M. Rossi, E. Roulleau, B. Suski, Xavier Rassion, and Etienne Wheris for their participation to the three field surveys and Alicia Hotovec for the compilation of the data. A special thanks to M. Marsella for providing us with the high resolution digital elevation model of Vulcano Island, J. Vandemeulebrouck and M. Todesco for fruitful discussions. We thank Eric Calais and two anonymous referees for their useful comments. IPGP contribution 2656.

References

Aubert, M., S. Diliberto, A. Finizola, and Y. Chébli (2008), Double origin of hydrothermal convective flux variations in the Fossa of Vulcano (Italy), *Bull. Volcanol.*, *70*, 743–751, doi:10.1007/s00445-007-0165-y.

Baldi, P., et al. (2002), Validation and comparison of different techniques for the derivation of digital elevation models and volcanic monitoring (Vulcano Island, Italy), *Int. J. Remote Sens.*, *23*(22), 4783–4800, doi:10.1080/01431160110115861.

Barde-Cabusson, S., et al. (2009), New geological insights and structural control on fluid circulation in the Fossa cone (Vulcano, Aeolian Islands, Italy), *J. Volcanol. Geotherm. Res.*, *185*, 231–245, doi:10.1016/j.jvolgeores.2009.06.002.

Blanco-Montenegro, I., R. De Ritis, and M. Chiappini (2007), Imaging and modelling the subsurface structure of volcanic calderas with high-resolution aeromagnetic data at Vulcano (Aeolian Islands, Italy), *Bull. Volcanol.*, *69*, 643–659, doi:10.1007/s00445-006-0100-7.

Chiodini, G., et al. (2005), Carbon dioxide diffuse degassing and estimation of heat release from volcanic and hydrothermal systems, *J. Geophys. Res.*, *110*, B08204, doi:10.1029/2004JB003542.

Frazzetta, G., L. La Volpe, and M. F. Sheridan (1983), Evolution of the Fossa cone, Vulcano, *J. Volcanol. Geotherm. Res.*, *17*, 329–360, doi:10.1016/0377-0273(83)90075-6.

Gambino, S., and F. Guglielmino (2008), Ground deformation induced by geothermal processes: A model for La Fossa Crater (Vulcano Island, Italy), *J. Geophys. Res.*, *113*, B07402, doi:10.1029/2007JB005016.

Gioncada, A., R. Mazzuoli, M. Bisson, and M. T. Pareschi (2003), Petrology of volcanic products younger than 42 ka on the Lipari Vulcano complex (Aeolian Islands, Italy): An example of volcanism controlled by tectonics, *J. Volcanol. Geotherm. Res.*, *122*, 191–220, doi:10.1016/S0377-0273(02)00502-4.

Granieri, D., et al. (2006), Correlated increase in CO_2 fumarolic content and diffuse emission from La Fossa crater (Vulcano, Italy): Evidence of volcanic unrest or increasing gas release from a stationary deep magma body?, *Geophys. Res. Lett.*, *33*, L13316, doi:10.1029/2006GL026460.

Italiano, F., P. M. Nuccio, and M. Valenza (1984), Mass geothermal energy release at Vulcano, Aeolian Islands, Italy, *Bull. Mineral. Rend. Soc. Ital. Mineral. Petrol.*, *39*, 379–386.

Johnson, T. C., R. J. Versteeg, A. Ward, F. D. Day-Lewis, and A. Revil (2010), Improved hydrogeophysical characterization and monitoring through high performance electrical geophysical modeling and inversion, *Geophysics*, in press.

Legaz, A., et al. (2009), A case study of resistivity and self-potential signatures of hydrothermal instabilities, Inferno Crater Lake, Waimangu, New Zealand, *Geophys. Res. Lett.*, *36*, L12306, doi:10.1029/2009GL037573.

Mazzuoli, R., L. Tortorici, and G. Ventura (1995), Oblique rifting in Salina, Lipari, and Vulcano islands (Aeolian Islands, southern Italy), *Terra Nova*, *7*, 444–452, doi:10.1111/j.1365-3121.1995.tb00540.x.

Nuccio, P. M., and A. Paonita (2001), Magmatic degassing of multicomponent vapors and assessment of magma depth: Application to Vulcano Island (Italy), *Earth Planet. Sci. Lett.*, *193*, 467–481, doi:10.1016/S0012-821X(01)00512-X.

Revil, A., D. Hermitte, E. Spangenberg, and J. J. Cochémé (2002), Electrical properties of zeolitized volcaniclastic materials, *J. Geophys. Res.*, *107*(B8), 2168, doi:10.1029/2001JB000599.

Revil, A., A. Finizola, F. Sortino, and M. Ripepe (2004), Geophysical investigations at Stromboli volcano, Italy. Implications for ground water flow and paroxysmal activity, *Geophys. J. Int.*, *157*(1), 426–440, doi:10.1111/j.1365-246X.2004.02181.x.

Revil, A., et al. (2008), Inner structure of La Fossa di Vulcano (Vulcano Island, southern Tyrrhenian Sea, Italy) revealed by high resolution electric resistivity tomography coupled with self-potential, temperature, and soil CO_2 diffuse degassing measurements, *J. Geophys. Res.*, *113*, B07207, doi:10.1029/2007JB005394.

Rücker, C., T. Günther, and K. Spitzer (2006), Three-dimensional modeling and inversion of DC resistivity data incorporating topography—I. Modelling, *Geophys. J. Int.*, *166*, 459–505, doi:10.1111/j.1365-246X.2006.03010.x.

A. Finizola, Laboratoire GéoSciences Réunion, UMR 7154, UR, IPGP, 15 avenue René Cassin, BP 7151, F-97715 Saint-Denis CEDEX 9, La Réunion.

T. C. Johnson, Energy Resource Recovery and Management, Idaho National Laboratory, PO Box 1625, Idaho Falls, ID 83415-2107, USA.

A. Revil, Department of Geophysics, Colorado School of Mines, 1500 Illinois St., Golden, CO 80401, USA. (arevil@mines.edu)